Reports

A Dynamical Instability of Spark-Ignited Engines

Abstract. *A simple model for spark-ignited engines is proposed in which the residual exhaust gases of a combustion event affect ignition of the subsequent charge. The model is an example of a one-dimensional, discrete, nonlinear mapping of an interval. Laminar flame correlations incorporated within models for ignition exhibit Arrhenius kinetics. Small variations of the ignition time with respect to the expansion cycle alter the work produced by each cycle, thereby altering the exhaust-gas temperature. It is shown that the mixing of hot residual gases with a fresh charge is a sufficient mechanism to produce an instability of the ignition process, resulting in oscillatory behavior. When this instability is compounded with the effects of mixture turbulence, one obtains a novel picture of the well-known phenomenon of "cyclic dispersion" exhibited by such engines.*

Spark-ignited internal combustion engines, as exemplified by the automobile engine, exhibit well-known variations in combustion rates (*1–5*). This apparently random behavior significantly degrades engine performance and confounds the task of engine tuning and control. Many factors contribute to this phenomenon, particularly mixture turbulence at the time of ignition. The purpose of this report is to demonstrate that a dynamical instability may also exist and may contribute to this behavior under certain operating conditions. The dynamical instability is induced by the coupling of nonlinear combustion kinetics with temperature and, consequently, with the thermodynamic engine cycle.

The phenomenon, known as "cyclic dispersion," is generally reported as a cycle-to-cycle variation in the maximum recorded pressure within an engine cylinder. The relative variation may range from 5 to 20 percent in well-tuned engines (*1*). The causes for the underlying variations in combustion rate are not well understood, although turbulence of the reaction mixture has been repeatedly suggested (*2, 3*). Factors that increase mixture turbulence or combustion flame speed tend to reduce the degree of dispersion. Shrouded inlet valves, for example, reduce the dispersion by half (*4*). The addition of inerts or exhaust-gas recirculation slows combustion flame speed and increases the degree of dispersion.

A significant problem has been to determine the effects of one engine cycle on the next. In a typical engine, 5 to 20 percent of the hot exhaust gases resulting from combustion remain within the cylinder to dilute the subsequent charge. If only every second charge is ignited (the intervening charge serving to purge the cylinder of exhaust gases), then a significant reduction in pressure dispersion is observed (*5*). This observation is supported by the results of experimental studies in which the throttle opening is used to alter the amount of exhaust gases (*2*). Patterson (*4*) also used skip-firing in an experimental investigation but altered the spark advance and throttle setting so as to maintain constant work per fired cycle. In this case, no change in cyclic dispersion was apparent. None of these investigations, however, seem conclusive because of the experimental difficulty associated with distinguishing the effects of residual gases, charge dilution, and spark timing.

The combustion process is initiated by a spark occurring during compression of a combustible mixture. An induction period is required in order to establish a flame front prior to the main combustion event (*6*). The periods of ignition delay and combustion are measured in the angular units of the engine cycle and are defined, respectively, as the intervals required to proceed from 0 to 1 percent and from 1 to 99 percent of complete combustion. These intervals, $\Delta\theta_{\rm ig}$ and $\Delta\theta_{\rm c}$, are correlated with the laminar flame speed, $S_{\rm l}$, by $(S_{\rm l})^{-2/3}$. Correlations for laminar flame speed exhibit a characteristic Arrhenius temperature dependence (*6*).

$$S_{\rm l} = kT_{\rm u}\left[\frac{1}{T_{\rm m}}\exp\left(\frac{-E_{\rm a}}{RT_{\rm m}}\right)\right]^{1/2} \qquad (1)$$

where $T_{\rm u}$ is the temperature of the unburned mixture, R is the gas constant, $E_{\rm a}$ is the activation energy, and $T_{\rm m}$ is a mean flame temperature given by

$$T_{\rm m} = T_{\rm u} + \epsilon'\,\Delta T_{\rm c} \qquad (2)$$

where $\Delta T_{\rm c}$ denotes the adiabatic temperature rise due to combustion, and ϵ is an averaging parameter. For the present purposes, $\Delta\theta_{\rm ig}$ and $\Delta\theta_{\rm c}$ are lumped as a single combustion delay, $\Delta\theta$. Instantaneous, complete combustion is assumed to occur at the end of the delay period. The delay is then correlated by the expression

$$\Delta\theta = kT_{\rm u}^{-2/3}\,T_{\rm m}^{1/3}\exp\left(\frac{E_{\rm a}}{3RT_{\rm m}}\right) \qquad (3)$$

An air standard Otto cycle is used to describe expansion and compression processes. Using $T_{\rm B}^j$ to denote the mixture temperature at the start of the jth compression cycle, we find that the gas temperature during ideal isentropic compression is given by $T(\theta) = T_{\rm B}^j/f(\theta)$, where

$$f(\theta) = \left[\lambda + (1-\lambda)\sin^2\frac{\theta}{2}\right]^{\gamma-1} \qquad (4)$$

and where λ is the inverse of the compression ratio, γ is a ratio of heat capacities, and θ is the crank angle with respect to the minimum volume position (top dead center).

The main events of a model engine cycle are summarized as follows:

1) $\theta = -\pi$. Compression starts. The mixture temperature is determined by the mixing of hot residual gases and fresh charge at ambient temperature, $T_{\rm amb}$. Thus, to a first order,

$$T_{\rm B}^j = r\,T_{\rm ex}^{j-1} + (1-r)T_{\rm amb} \qquad (5)$$

where r represents the fraction of residuals.

2) $\theta = \theta_{\rm s} < 0$. A spark is introduced to initiate combustion. The mixture temperature is $T_{\rm s}^j = T_{\rm B}^j/f(\theta_{\rm s})$. The combustion delay is determined by Eq. 3 with mean flame temperature

$$T_{\rm m}^j = T_{\rm s}^j + \epsilon(1-r)\Delta T \qquad (6)$$

3) $\theta = \theta_{\rm s} + \Delta\theta^j$. Complete, instantaneous combustion occurs to yield a mixture temperature

$$T_{\rm c}^j = \frac{T_{\rm B}^j}{f(\theta_{\rm s} + \Delta\theta^j)} + (1-r)\Delta T \qquad (7)$$

where

$$\Delta\theta^j = k(T_{\rm s}^j)^{-2/3}\,(T_{\rm m}^{j1/3}\exp\left(\frac{E_{\rm a}}{3RT_{\rm m}^j}\right) \qquad (8)$$

4) $\theta = +\pi$. Adiabatic expansion of the combustion mixture yields an exhaust-gas temperature,

$$T_{\rm ex}^j = f(\theta_{\rm s} + \Delta\theta^j)T_{\rm c}^j \qquad (9)$$

These individual steps constitute a simple, one-dimensional model for an ideal engine cycle. Given a value for $T_{\rm ex}^j$, Eqs. 3 through 9 may be used to compute the subsequent value $T_{\rm ex}^{j+1}$. Thus the

Table 1. Parameter values for the curves illustrated in Figs. 1 through 3. The parameters were chosen in accordance with published data for kinetic models (*1–6*).

Figure	Residual recycle, r	Adiabatic temperature rise due to combustion, ΔT (K)	Activation energy, E_a (cal)	Compression ratio, $1/\lambda$	Averaging parameter, ϵ	Ambient temperature, T_{amb} (K)	Kinetic constant, k ($K^{1/3}$)	Spark position, θ_s (rad)
1	0.15	1700	38,600	8	0.74	300	0.2	−0.5
2 and 3	0.20	2000	44,700	12	0.50	300	0.1	−1.5

model has the general form of a recursion relation, $T^{j+1}_{ex} = g(T^j_{ex})$. The model may also be presented graphically as a plot of T^{j+1}_{ex} versus T^j_{ex}. Figures 1 and 2 illustrate such plots for the model parameters listed in Table 1. The intersection of the graph of $g(T^j_{ex})$ with the diagonal marks a value of T^j_{ex}that remains unchanged upon iteration of the model, that is, a stationary steady state.

The stability of a stationary steady state for a one-dimensional recursion mapping is determined by the slope of the map at steady state. The steady state $T_{ex} = g(\overline{T}_{ex})$ is stable if $-1 < g'(\overline{T}_{ex}) < 1$ (an overbar denotes a steady-state value). For the case of the recursion mapping represented by Eqs. 3 through 9, the slope is negative if $E_a > R\overline{T}_m$. Normally E_a is an order of magnitude larger than $R\overline{T}_m$; thus only the lower bound on $g'(\overline{T}_{ex})$ is significant. Some algebraic manipulation yields the following criterion for asymptotic stability of the stationary steady state:

$$\Delta T \left(\frac{E_a - RT_m}{3RT^2_m} + \frac{2}{3T_s} \right) \leq \frac{(1 + r) f(\theta_s)}{r(1 - r) f'(\theta_c)(\theta_c - \theta_s)} \qquad (10)$$

The right side of Eq. 10 depends only on design parameters for the engine, including the timing of the spark and combustion events, the compression ratio, and the fraction of residual gases retained on each cycle. To enhance stability, the designer could decrease the compression ratio or reduce the amount of recycled residual gases. Function $f(\theta)$ exhibits a minimum at $\theta = 0$, that is, $f'(0) = 0$, so that timing the combustion event to occur near top dead center would also enhance stability.

The left side of Eq. 10 contains various kinetic constants, including the adiabatic temperature rise due to combustion, activation energy for combustion, and steady-state values of the mean flame temperature and spark gas temperature. The activation energy is the dominant term and largely controls the onset of oscillatory behavior. The relative importance of ΔT is ameliorated by the linear dependence of $\overline{T}_m$ on ΔT. In fact, extreme values of ΔT could serve to induce stability.

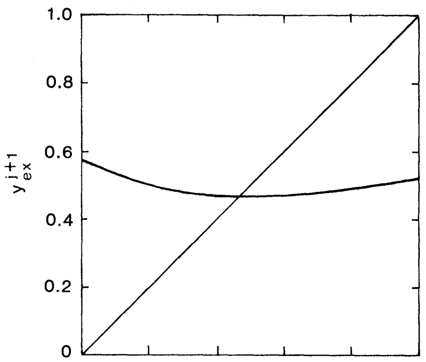

Fig. 1 (top). Dimensionless exhaust-gas temperature y_{j+1} versus y_j. Plotted are the dimensionless values $y_j = (T^j_{ex} - T^j_{amb})/\Delta T$. Starting with an initial value for y_0, one can use the graph to determine y_1. Using the graph again, y_2 may be found. Continued iteration yields the sequence $y_0, y_1, y_2, \ldots$. A point at the intersection of the curve $y_{j+1} = g(y_j)$ with the diagonal represents a steady state for the iterative process. For the case presented in this figure, all sequences asymptotically approach the steady state, thereby indicating dynamical stability.

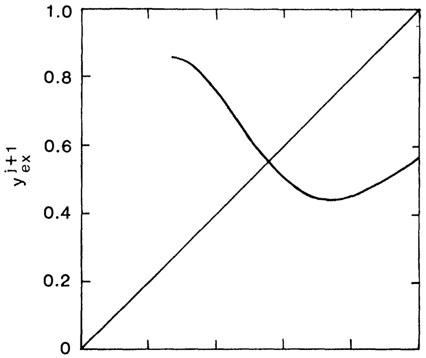

Fig. 2 (middle). Dimensionless exhaust-gas temperature y_{j+1} versus y_j for an unstable steady state. Parameters are taken from Table 1.

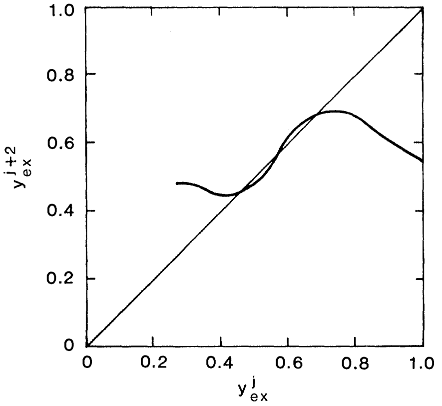

Fig. 3 (bottom). Dimensionless temperature y_{j+2} versus y_j. Intersections with the diagonal indicate values of y that are repeated every second step of the iteration process, thereby representing oscillatory dynamics. Parameters are the same as for Fig. 2.

Figure 1 illustrates the case of a single, stable steady state. By contrast, the steady state of Fig. 2 is unstable and results in oscillatory behavior. This is more clearly shown in Fig. 3, which is constructed by computing

$$T^{j+2}_{ex} = g(T^{j+1}_{ex}) = g(g(T^j_{ex})) \qquad (11)$$

An intersection with the diagonal in Fig. 3 marks a value of T^j_{ex} that is encountered on every second cycle, resulting in a limit cycle of period two.

Figure 3 also demonstrates the almost neutral stability of the oscillatory state. Perturbations of the exhaust-gas temperature result in long transient excursions from the nominal limit-cycle behavior. Consequently, such systems would be sensitive to external fluctuations.

The simple, one-dimensional model suggested herein is an example of iterative, discrete time dynamics (*7*). Schmitz and his co-workers proposed such a model for a loop reactor (*8*). In a recent thesis, Le studied one- and two-dimensional discrete models for batch reactors with partial recycle (*9*). A full range of complex dynamical behavior was observed, including long limit cycles and chaos. Further experimental and modeling work will be required to determine if the spark-ignited engine belongs to this class of complex systems.

JEFFREY C. KANTOR
Department of Chemical Engineering,
University of Notre Dame,
Notre Dame, Indiana 46556

References and Notes

1. M. B. Young, *SAE Pap. 810020* (1980), pp. 1–25.
2. G. Karim, *J. Inst. Pet. (London)* **53**, 519 (1967).
3. R. E. Winsor and D. J. Patterson, *SAE Pap. 730086* (1973).
4. D. J. Patterson, *SAE Pap. 660129* (1967), p. 621.
5. J. P. Soltau, *Proc. Inst. Mech. Eng. (Automotive Div.)* (No. 2), 99 (1960).

6. S. D. Hires *et al.*, *SAE Pap. 780232* (1978), p. 1053.
7. R. M. May, *Nature (London)* **261**, 459 (1976); P. Collet and J.-P. Eckmann, *Iterated Maps on the Interval as Dynamical Systems* (Birkhauser, Boston, 1980); C. Preston, *Iterates of Maps on an Interval* (Springer-Verlag, New York, 1983).
8. M. J. Reilly and R. A. Schmitz, *AIChE J.* **12**, 153 (1966); R. B. Root and R. A. Schmitz, *ibid.* **15**, 670 (1969).
9. N. B. Le, thesis, University of Notre Dame (1982).

10. Supported by NSF grant CPE83-07293-01 and by the Henry and Camille Dreyfus Foundation.

16 November 1983; accepted 9 April 1984

Copepod Fecal Pellets as a Source of Dihydrophytol in Marine Sediments

Abstract. *Dihydrophytol (3,7,11,15-tetramethylhexadecanol) was identified in the nonsaponified lipid fraction of fecal pellets from the copepod* Calanus helgolandicus *fed in the laboratory on a unialgal diet. Direct deposition in the fecal pellets of certain zooplankton species may explain the presence of dihydrophytol in marine sediments. Microbial reduction of phytol in sediment cores does not account for the origin of this compound in all sedimentary environments.*

Phytol [3,7(*R*),11(*R*),15-tetramethylhexadec-2(*E*)-enol], the ester-linked isoprenoid side chain of chlorophylls a and b, is an important and abundant algal lipid. It is recognized as the precursor of a variety of acyclic isoprenoid compounds of 20 or fewer carbon atoms detected in aquatic organisms (*1–3*) and bottom sediments (*4*).

Sever and Parker (*5*) first detected dihydrophytol (3,7,11,15-tetramethylhexadecanol) in aquatic sediments and suggested that it was formed by hydrogenation of phytol under reducing conditions. Speculation was not made as to what mediates this reduction. Other researchers (*6, 7*) subsequently noted dihydrophytol in freshwater, estuarine, and marine sediments and proposed rapid microbial reduction of phytol in the surfacemost sediment as its most likely derivation.

We now report that dihydrophytol can be directly introduced into particular sediments through the deposition of fecal pellets released by certain species of zooplankton. In situ microbial production from phytol (*8*) is not a requirement for the presence of this compound in all aquatic sediments.

Controlled feeding experiments were carried out in the laboratory with two different species of zooplankton, stage 5 of the copepod *Calanus helgolandicus* and nauplii of the barnacle *Elminius modestus*. The copepods were collected fresh by tow net and the nauplii were from adults obtained in the sea area of Plymouth Sound, England. Fecal pellets were obtained from an experiment in which the copepod and the barnacle nauplii were individually fed the green alga *Dunaliella primolecta* and from an experiment in which the copepod was fed the same alga but with both organisms treated overnight with antibiotics (benzopenicillin and streptomycin, each 50 mg/liter) before the start of feeding. Each experiment was conducted over a period of 1 day, after which the fecal pellets, animals, and uneaten algal cells were separated by sequential filtering through nylon meshes (*9, 10*).

All samples, including a portion of the original algal food stock, were then collected on combusted glass fiber filters and stored under methanol in a freezer until chemical extraction (*11*). Before storage, the animals were transferred to filtered seawater and starved overnight to eliminate any gut contents; half of the fecal pellet sample obtained from each of the two copepod experiments was transferred to stoppered glass tubes containing oxic, filtered seawater and aged for 2 weeks at 10°C.

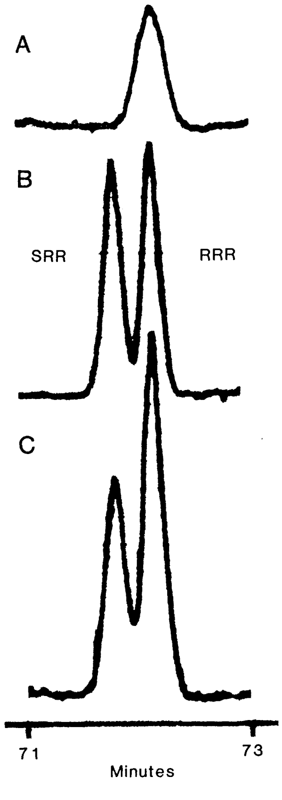

Fig. 1. Stereochemistry of dihydrophytol in copepod fecal pellets. (A) The total alcohol fraction of the untreated, unaged copepod fecal pellet sample, chromatographed as acetate derivatives on a polar glass capillary column [DEGS/PEGS, 50 m by 0.3 mm (inner diameter)] with hydrogen carrier gas (1.8 kg/cm^2) and temperature programming (20° to 125°C at 4°C per minute), yields a single peak for dihydrophytol. (B) A 1:1 mixture of *SRR* and *RRR* isomers, made by reducing commercial phytol with hydrogen and PtO_2 as catalyst, resolves into its two diastereomeric components under these chromatographic conditions. (C) The dihydrophytol of the sample coinjects with the second eluting component (*RRR*) of the standard mixture. Although the *SSS* enantiomer represents a possible structural assignment, the *RRR* configuration is assigned in view of the 2(*E*),7(*R*),11(*R*) stereochemistry of algal phytol.

Results of the analyses of the total fatty alcohol fractions (*12*) of the alga and of each pellet sample are summarized in Table 1. Phytol was the only alcohol detected in the alga (*9*). It also dominated the total fatty alcohol composition in the copepod (*9*) and barnacle nauplii pellets. Phytol was not detectable in the total alcohol fraction of either animal, even with multiple ion detection gas chromatography–mass spectrometry, although calanid copepods are known to accumulate metabolites of phytol in their total lipid pool (*13*). Dihydrophytol was observed only in the copepod pellets and not in those of the barnacle nauplii, in either animal, or in the algal diet. The presence of dihydrophytol in copepod fecal pellets and its absence from the algal diet strongly suggests that it is a metabolite of dietary phytol in this animal.

The stereochemistry of the dihydrophytol in the fecal pellets was determined by gas chromatography (Fig. 1) and is designated as 3(*R*),7(*R*),11(*R*),15-tetramethylhexadecanol. The presence of only one isomer of dihydrophytol is consistent with its formation through a biologically controlled reduction of the double bond of phytol (*6*). An abiotic reduction would occur nonstereospecifically and yield an approximately equal mixture of *SRR* and *RRR* isomers (*14*).

Our observation of dihydrophytol in the fecal pellets of *C. helgolandicus* fed a unialgal diet demonstrates that in situ microbial production from phytol is not the only process responsible for the appearance of this compound in sediment deposits. Van Vleet and Quinn (*7*) suggested that the exclusively *RRR* isomer of dihydrophytol observed in recent sediments from the Gulf of Maine is formed